ISSN 1533-9211

DOI 10.17605/OSF.IO/JRQA5

MTI IMPROVEMENT FACTOR ENHANCEMENT AND RADAR SYSTEMS PERFORMANCE BY USING DOUBLE –DELAY FILTER AT THREE –PERIOD STAGGERED

MOHAMMED JASIM AL- SUMAIDAEE

PhD Student, Department of ECE, KL University, India.

M. SIVA GANGA PRASAD

Professor, Department of ECE, KL University, India.

DHAHIR ABADULHADE ABDULAH

Professor, Department of Computer, College of Science, University of Diyala, Iraq.

Abstract

Staggering the pulse repetition intervals is widely used to alleviate the blind speed problem in Moving Target Indication (MTI) radar systems. It is possible to increase the first blind speed on the order of ten solds using non-uniform sampling. Improvement in blind speed results in passband fluctuations that may degrade the detection performance for particular Doppler frequencies. Therefore, it is essential to design MTI filters with non-uniform interpulse periods with minimum passband ripples, sufficient clutter attenuation, and good range and blind velocity performance.

Keywords: Filter, Frequency, Response, Doppler, Processing, MTI, Clutter, Impulse, Response, PRF

INTRODUCTION

The design of the MTI processor is mainly based on the design of filter structure for clutter attenuation. For stationary clutter attenuation, simple highpass filters provide sufficient attenuation, whereas higher-order filters can be required to sufficiently attenuate clutter with significant Doppler spread [1].

Design of staggered MTI filters depends upon the radar system parameters that are related to the detectation probability and clutter attenuation based upon, staggered MTI filter design comprises on the optimization of two sets of parameters: the inter pulse time duration and the filter coefficients. The unambiguous range and velocity specifications impose constraints on the interpulse period. The desiered clutter attenuation affects the values of filter coefficients [2].

It is difficult to distinguish a moving target in a ground-clutter or sea-clutter environment due to strong clutter echos. Detection of moving targets in these conditions is performed using Moving Target Indication (MTI) radar. The MTI radar is a type of pulse radar that uses the non-zero Doppler shift of moving targets for their detection [3] by cancelling the stationary background clutter.

The Seybold Report
ISSN 1533-9211
DOI 10.17605/OSF.IO/JRQA5

Different types of MTI Radars are classified according to operation modes, environments and used signal processing algorithms. Coherent MTI Radar is the type in which a moving target is detected as a result of pulse-to-pulse change in the echo phase relative to the phase of a coherent reference oscillator [4]. In other words, it is a system that uses the phase difference resulting from the Doppler Effect to separate the moving targets from stationary background clutter. Pulses are transmitted and received echos are compared with the signal produced by the coherent reference oscillator. Due to Doppler shift, the moving target component of the received echo has a phase difference compared to the reference oscillator signal and can be discriminated from clutter [5].

Another type of MTI radar that uses the clutter echo as the reference signal to discriminate the Doppler-shifted information of target echo is known as Non-Coherent MTI or externally Coherent MTI [6]. This type of MTI is simpler than coherent MTI, but it requires the presence of clutter for detecting the moving targets. Due to clutter dependence, Non-Coherent MTI implemented as a mode and can be switched on or off depending on the presence or absence of strong clutter reference. [6].

1. Implementation of MTI system in Rader sets

One respect in which clutter masses differ from actual targets in that they move at different relative speeds. In the MTI system, the velocity characteristics conveyed by the doppler shift are used to distinguish the desired from undesired returns [7]. This is accomplished by employing filter networks (or their equivalent), which annul the returns from fixed targets bearing no Doppler shift while passing the frequency-shifted echoes from moving targets. Therefore, clutter elimination by these means is feasible to the extent that the energy spectrum returned by the cluttered mass is distinguishable from that of the target [8]. This is seldom the case. Either because of random fluctuations in scattering cross-section or random notions within the cluttered mass, the power spectrum occupies a continuous range of frequencies. Those components in the vicinity of the target frequencies are indistinguishable from target energy. Thus, depending on the width of the clutter spectrum about the range of target velocities to be accepted, a residue of uncancelable clutter persists [9].

2. Instability of Equipment

The effect of equipment instability on MTI performance depends upon the particular configuration of the radar [8, 10].

The performance of MTI radar will deteriorate if the transmitter, the Stalo, or the Coho drift in frequency, if the time delay in delay line does not equal the pulse repetition interval, if there are variations in pulse width or pulse amplitude, or if the transmitter frequency changes during the pulse [8-11].

Some of the sources of this noise are controllable up to a point in the design stage by calling for intrinsically stable components, providing automatic stabilizing circuitry, etc., in manufacturing, tightening critical tolerances, etc., and in the field, by ensuring careful maintenance, such procedure, however, become progressively more expensive. A compromise

ISSN 1533-9211

DOI 10.17605/OSF.IO/JRQA5

is usually reached, with the result that a certain amount of instability noise remains to degrade the MTI performance [11-14].

3. Internal Fluctuation of Clutter

Although clutter targets such as buildings, water towers or mountains produce echo signals that are constant in both phase and amplitude as a function of time, many clutter types cannot be considered stationary. Echoes from trees, sea, rain and chaff fluctuate with time, and those fluctuations can limit the performance of MTI radar [15].

Because of its varied nature, it is difficult to describe precisely the clutter echo signal. However, for analysis, most fluctuating clutter targets may be represented by a model consisting of many independent scatterers within the radar's resolution cell.

The echo at the radar receiver is the vector sum of the echo signals received from each scatterer. That is each scatterer's relative phase and amplitude influence the resultant composite signal. If the individual scatterers remain fixed from pulse to pulse, the resulting echo signal will also remain fixed [16].

4. Wind Noise

The decorrelation effect of particle motion describes the impact of partial motion relative to the centre of gravity of the cluttered mass. This agitation may be primarily [17].

Due to wind, the standard deviation parameter will have to be chosen accordingly [18]. For ground clutter, the centre of gravity of the cluttered mass will be fixed regarding minor wind velocity; however, for airborne clutter such as rain, clouds and chaff. The centre of gravity will drift at the wind velocity, Vw, concerning the ground. If the rate is steady, this drift will produce a Doppler shift of the entire clutter spectrum away from the central ground-clutter frequency by an amount:

$$f_w = \frac{2V_w}{\lambda} \qquad (1)$$

For eliminating the wind noise, it has been seen that in noncoherent systems, wind decorrelation will not be present. Similarly, it can be removed in coherent system, if the Coho can be adjusted (as a function of beam position) so as to "zero beat" on the center of the returned clutter spectrum, and to find the clutter line spectrum in presence of wind, we have table (1) which indicates the speed in km/h, and the standard deviation of wind with wave lengths.

Speed of wind in	Standard Deviation of Wind
km/h	$\delta_w.\lambda(m/s)$
18.3	0.8
36.3	4.5
37.5	6.5

Table 1: Represents a Speed of Wind (km/h), With Standard Deviation of Wind and Wavelength in (m/s)

The Seybold Report
ISSN 1533-9211
DOI 10.17605/OSF.IO/JRQA5

5. Scanning of the Antenna

When the radar beam is scanned over a broad search sector by mechanical rotation of the antenna or other means, the spectral spread of the received clutter signals increases, the increase can be attributed to the amplitude modulation of the echo signal by the two-way beam pattern or, equivalently, to the introduction of an added velocity component by the motion of the antenna. Assuming the usual idealized clutter target, the echo signal will consist of the vector sum of the contribution from many independent scatterers randomly distributed within the radar resolution cell. Because the scatterers are considered independent, the received echo power is equal to the sum of the average power scattered by each object [19-20].

The scanning motion of the antenna causes the beam to shift to a slightly different azimuth on each pulse [21]. Most scatterers remain within the shaft. Some scatterers are no longer illuminated, while others enter the beam and become illuminated [22]. The result is that the total number of illuminated scatterers will be the same from pulse to pulse. Still, their relative distribution in space and their relative phase relations will be different [23]. Therefore, the resultant echo signal voltage varies from pulse to pulse, and an uncancelled residue remains at the output of the delay line canceller. In other words, the antenna scanning influences the shape of the clutter spectrum. Each scatterer provides an echo which exhibits the same spectral characteristics as a point target. In-ground clutter theory, scattering elements are assumed to be independent. Therefore, the resulting spectrum is the sum of the spectra of the individual scatterers and has the same shape as that of the target [24].

A method for eliminating scanning noise is called (step-scanning). The step scanning antenna is held (electronically) fixed through the prescribed time interval, Δt, assigned to each direction. In this way the reflected echoes will be modulated by a rectangular function, the truncation points of which are known. If the two-pulse comparison, delay time is used, the return pulses from fixed targets will be canceled, with the exception of the first and last pulses. These uncancelled pulses can then be eliminated by blanking the display during the range frames immediately following the antenna steps similarly [25-27].

6. Platform-motion Noise

When the radar itself is in motion, as with a shipboard or airborne radar, detecting a moving target in the presence of clutter is more complex than if the radar were stationary [28]. In this case, additional noise is introduced into the system. As to origin, this platform noise is distinct from the internal fluctuation of wind and scanning noises previously described; however, it has elements of similarity with each. As fixed particles drift through the antenna beam pattern, they are scanned, and acertain amount of scanning noise results. This noise will be generated when the antenna is sighted at (90°) to the ground track and will be worse for narrow than for broad-beam patterns; if the antenna is sighted forward or afterwards, the scanning noise will be small, but in this case, the fixed particles will drift through the range resolution intervals, producing what might be called (ranging noise). Both the scanning and the ranging noise can be accounted for in the analysis by appropriately limiting the integration time [29].

ISSN 1533-9211

DOI 10.17605/OSF.IO/JRQA5

The unified relative motion of the fixed clutter mass can be decomposed into a translation and a rotation, each producing a characteristic noise. The translation noise is the same as the wind noise. It is unimportant for noncoherent systems (and coherent systems in which the Coho frequency can be adjusted as a function of sighting angle and ground speed). The rotation noise, on the other hand, can be very serious. Let the antenna be sighted at an angle concerning the ground track, as shown in Fig.1. Let the aircraft velocity be V, and consider a fixed particle at p, in the rth range –resolution interval making an angle, with the beam axis. To the moving observer, the cluttered mass will appear to rotate above the point, (0), at an angular rate w given by:

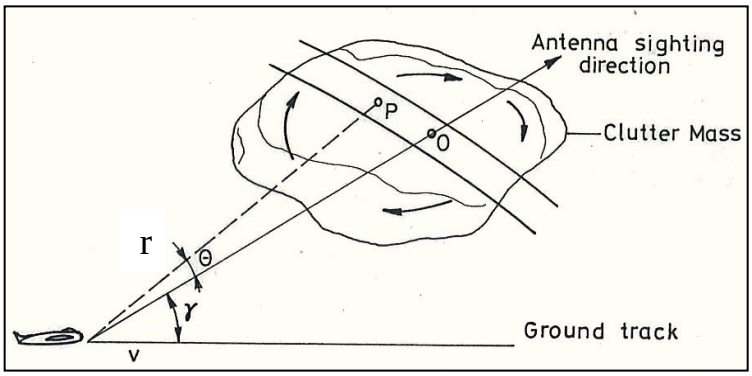

Figure 1: Relative Rotation of Clutter Mass due to Platform Motion

$$W = \frac{V \sin \gamma}{r} \quad (2)$$

Consequently, the particle at p, will exhibit a relative radial velocity, Vp, which for small beam width is approximately

$$V_p = wr\theta \quad (3)$$

$$V_p = V_\theta sin\gamma \quad (4)$$

The voltages returned from a reflector at p will be spectrally distributed around the Doppler shift frequency corresponding responding toV_p, i, e,

$$f_d = \frac{2V_P}{\lambda} \quad (5)$$

$$f_d = \frac{2v\theta \sin \gamma}{\lambda} \quad (6)$$

For equipment of lower resolution capability, the range noise will be less severe, and, fortunately, it will diminish as the sighting angle increases, i.e. in contrast. To the rotation noise, which is most severe for $\gamma = 90^o$.

Since both the scanning and ranging noise can be accounted for by integrating the correct number of hits per target the platform-motion noise will be presumed to be entirely due to rotation.

ISSN 1533-9211

DOI 10.17605/OSF.IO/JRQA5

7. How to generate a stegger Prf.

A three period stagger can be obtained with the same circuitry as that for two period stagger. The only alteration is the timing of the electronic switch, a switch is left in the upper position for two pulses and then moved down for one.

The three pulse intervals now have a ratio:

(Ti – ΔT); Ti; (Ti – ΔT) as shown in Fig (5)

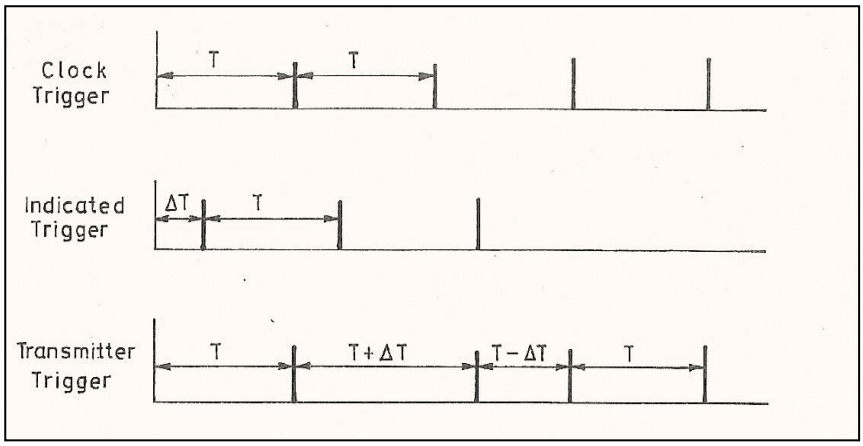

Figure 2: Three-Period -Stagger Ratio

(Ti – ΔT); Ti; (Ti – ΔT)

This operation is shown in Fig. (3) With its necessary block diagram.

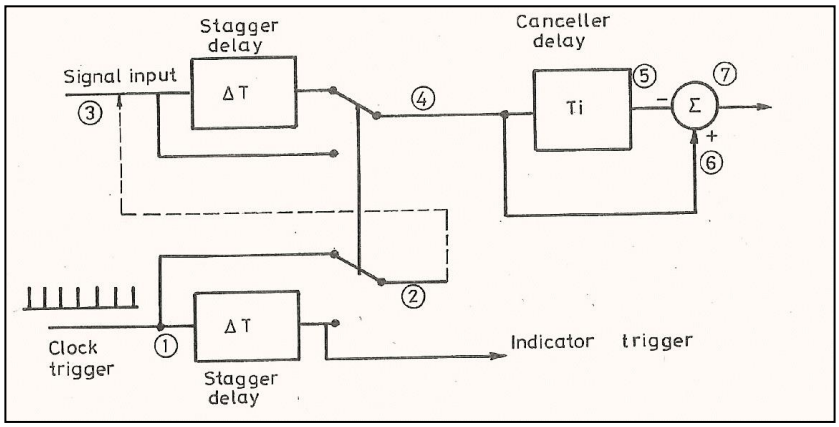

Figure 3: Block Diagram for Generating Staggered PRF

8. Frequency Response Charateristies

For deriving the expression of frequency response characteristics therefore, the envelop is sampled at times:

The Seybold Report
ISSN 1533-9211
DOI 10.17605/OSF.IO/JRQA5

to + nT ….. For n even

And

to + nT + ΔT ….. For n odd

But for all n will be:

$$tn = to + \frac{\Delta T}{2} + nt + (-1)^n \frac{\Delta T}{2} \quad (7)$$

The Amplitude of nth pulses is:

$$An = Sin\ 2\pi fd\ \left(to + \frac{\Delta T}{2} + nT + (-1)^n \frac{\Delta T}{2}\right) \quad (8)$$

Where:

An: amplitude of nth pulses

To = total time of pulses

ΔT= stagger delay

T = Period time

By putting

$$t_1 = to + \frac{\Delta T}{2} \quad (9)$$

Expanding the expression will be:

$$An = Sin\ 2\pi f_d\ (t_1 + nT).Cos2\pi f_d(-1)^n \frac{\Delta T}{2} + Cos\ 2\pi f_d\ (t_1 + nT).Sin2\pi f_d(-1)^n \frac{\Delta T}{2}$$

$$An = Sin\ 2\pi f_d\ (t_1 + nT).Cos2\pi f_d(-1)^n \frac{\Delta T}{2} + (-1)^n\ Cos2\pi f_d(t_1 + nT)Sin\ 2\pi f_d.\frac{\Delta T}{2}$$

For n integer, $(-1)^n = Cosn\pi \therefore\ Cos(-n\pi) =\ \ Cosn\pi$

For Three period Stagger

The nth sample is taken at

To + nT + ΔT

∴(n+3) th at ….. to + (n+3) T + ΔT…

Successive Period

T-ΔT, T, T + ΔT

∴The Function Will be has This Property

ISSN 1533-9211

DOI 10.17605/OSF.IO/JRQA5

$$\left(\frac{1}{3}+\frac{2}{3}Cos\frac{2n\pi}{3}\right) \quad (10)$$

$$\therefore \left(\frac{1}{3}+\frac{2}{3}Cos\frac{2n\pi}{3}+\frac{1}{6}-\frac{1}{6}\right)$$

$$\left(\frac{1}{2}+\frac{2}{3}Cos\frac{2n\pi}{3}-\frac{1}{6}\right)=\left(\frac{1}{2}+\frac{2}{2}.\frac{2}{3}Cos\frac{2n\pi}{3}-\frac{1}{6}\right)$$

$$\frac{1}{2}\left(1+\frac{4}{3}Cos\frac{2n\pi}{3}-\frac{1}{3}\right)$$

This expression takes the values

+1, -1, -1, +1, …… For n integer

It has been supposed before

$$t_{1=}to+\frac{\Delta T}{2} \quad (11)$$

$$\therefore An=sin2\pi f_d\left\{to+nT+\frac{\Delta T}{2}\left(\frac{4}{3}Cos\frac{2n\pi}{3}-\frac{1}{3}\right)\right\} \quad (12)$$

$$An=sin2\pi f_d\left\{t_1+nT+\frac{1}{2}\left(\frac{4}{3}Cos\frac{2n\pi}{3}-\frac{1}{3}\right)\frac{\Delta T}{2}\right\}$$

$$An=sin2\pi f_d(t_1+nT)Cos2\pi f_d\left(\frac{4}{3}Cos\frac{2n\pi}{3}-\frac{1}{3}\right)\Delta T+$$

$$Cos2\pi f_d(t_1+nT)sin\pi f_d\left(\frac{4}{3}Cos\frac{2n\pi}{3}-\frac{1}{3}\right)\Delta T$$

$$An=sin2\pi f_d(t_1+nT)Cos2\pi f_d-\frac{1}{3}Cos2\pi f_d(t_1+nT)sin\pi f_d\Delta T$$

$$+\frac{4}{3}Cos2\pi f_d(t_1+nT)Cos\frac{2n\pi}{3}sin\pi f_d\Delta T$$

$$An=sin2\pi f_d(t_1+nT)Cos\pi f_d\Delta t-\frac{1}{3}Cos2\pi f_d(t_1+nT)sin\pi f_d\Delta T$$

$$+\frac{4}{3}\left[\frac{1}{2}\left\{cos\,2tfd(t_1+nT)+\frac{2n\pi}{3}+cos\,(2\pi fd(t_1+nT)-\frac{2n\pi}{3}\right\}\right] \quad (13)$$

$$As\quad -Cos(2\pi f_d(t_1+nT)+\frac{2n\pi}{3}) \quad (14)$$

Suppose:

$$Cos2\pi\left(f_dt_1+f_dnT+\frac{n}{3}\right)$$

$$\therefore os2\pi\left(f_dt_1+f_dnT+\frac{n}{3}\right)\equiv Cos2\pi f_d(t_1+nT+\frac{n}{2f_d})$$

The Seybold Report
ISSN 1533-9211
DOI 10.17605/OSF.IO/JRQA5

$$\therefore Cos2\pi f_d(t_1 + nT + \left(1 + \frac{1}{3Tf_d}\right) = Cos2\pi f_d(t_1^1 + nT)$$

$$\therefore f_d\left[t_1 + nT\left(1 + \frac{1}{3Tf_d}\right)\right] = f_1(t_1^1 + nT)$$

$$\therefore f_d t_1 = f_1 t_1^1$$

And

$$f_d nT\left(1 + \frac{1}{3Tf_d}\right) = f_1 nT$$

$$\therefore f_d\left(1 + \frac{1}{3Tf_d}\right) = f_1$$

Where $fr = \frac{1}{T}$

$$\therefore f_1 = f_d + \frac{fr}{3} \quad (15)$$

Therefore:

$$An = Sin2\pi f_d(t_1 + nT)Cos\pi f_d\Delta T - \frac{1}{3}Cos2\pi f_d(t_1 + nT)sin\pi f_d\Delta T$$

$$+\frac{2}{3}Cos2\pi\left(f_d + \frac{fr}{3}\right)(t_1 + nT)Sin\pi f_d\Delta T + \quad (16)$$

$$\frac{2}{3}Cos2\pi\left(f_d - \frac{fr}{3}\right)(t_1 + nT)Sin\pi f_d\Delta T$$

Thr r.m.s canceller o/p for three-period stagger will be:

$$Vout = \left[G^2(f_d)\left(Cos^2\pi f_d\Delta T + \frac{1}{9}Sin^2\pi f_d\Delta T\right) + G^2\left(f_d + \frac{fr}{3}\right)\frac{4}{9}Sin^2\pi f_d\Delta T + G^2\left(f_d - \frac{fr}{3}\right)\frac{4}{9}Sin^2\pi f_d\Delta T \ldots\right]$$

For double cancellation G (f_d) = $Sin^2\ \pi f_d$ T

The r.m.s Canceller output will be:

$$|H_S(V)|^2 = sin^4\pi f_d T\left(Cos^2\pi f_d\Delta T + \frac{1}{9}Sin^2\pi f_d\Delta T\right) +$$

$$sin^4\left(\pi f_d T + \frac{\pi}{3}\right)\frac{4}{9}Sin^2\pi f_d\Delta T + sin^4\left(\pi f_d T - \frac{\pi}{3}\right)\frac{4}{9}Sin^2\pi f_d\Delta \quad (17)$$

The two previous expressions represent the reponse of MTI system for targets of different speeds finally putting:

$$|H_S(V)|^2 = sin^4\pi f_d T\left(Cos^4\pi f_d\Delta T\frac{M}{N} + \frac{1}{9}Sin^2\pi f_d\frac{M}{N}\right)$$

ISSN 1533-9211

DOI 10.17605/OSF.IO/JRQA5

$$+\frac{4}{9}sin^4\pi\left(f_dT+\frac{1}{3}\right)Sin^2\pi f_d\frac{M}{N}+\frac{4}{9}sin^4\pi(f_dT-\frac{1}{3})Sin^2\pi f_d\frac{M}{N} \quad (18)$$

For the Purpose of Computation this latter expression is more conveniently written after simplifying as:

$$|H_S(V)|^2=sin^4\pi f_dT-\frac{4}{3}Sin^2\pi f_dT\frac{M}{N}Sin^4\pi f_dT+\frac{1}{2}Sin^2\pi f_dT\frac{M}{N} \quad (19)$$

The expression before can computed and plotted of angle (πf_dT) for agiven values $\left(\frac{\Delta T}{T}\right)or\left(\frac{M}{N}\right)$

Where M= Stagger delay

N= Canceller delay

A forming of computer program is done for Eq. (19) and for six cases by choosing the mean period of main delay line (N) as (5,10,15,20,25 and 30) and changing the staggered delay (M) for each case from (1) to (M= N-1), to be able to analyse and predict the optimum case of staggering.

9. Double- Delay MTI Filter With Three Period Staggered:

The expression of frequency response characteristics for three period staggered has been obtained the expression (19).

$$|H_s(v)|^2=\sin^4(\pi Tf_d)-\frac{4}{3}\sin^2(\pi Tf_d\frac{M}{N})\sin^4(\pi Tf_d)+\frac{1}{2}\sin^2(\pi Tf_d\frac{M}{N})$$

A forming of computer program is done for (19) and for six cases by choosing the mean period of main delay line (N) as (5, 10, 15, 20, 25 and 30) and changing the staggered delay (M) for each case from (1) to (M= N-1), to be able to analyse and predict the optimum case of staggering. By employing the expression (19), which indicates the frequency response characteristic in case of three- period staggered and assuming that:

$$\pi T=a$$

$$\pi T\frac{M}{N}=b$$

By applying the definition of average gain to get:

$$\overline{G}=\frac{T}{N}\int_0^{N/T}(\sin^4 af-\frac{4}{3}\sin^2 bf\sin^4 af+\frac{1}{2}\sin^2 bf)df \quad (20)$$

Simplifying this expression to obtain

$$\overline{G}=\frac{T}{N}\int_0^{N/T}(1/3\cos 4af_d-4/3\cos 2af_d+3+2/3\cos bf_d\cos 4af_d-8/3\cos 2bf_d\cos 2a)df_d \quad (21)$$

The Seybold Report
ISSN 1533-9211
DOI 10.17605/OSF.IO/JRQA5

Solving this integral by supposing (M) and (N) are integers, we obtain

G = 3

Incast to obtain the expression of the improvement factor for three- period stagger.

From the definition of the improvement factor it has got:

$$I = G\frac{C_i}{C_0} \tag{22}$$

Where C_i is the clutter at the input of MTI filter and equal

$$C_i = \int_0^{\infty} e^{\frac{-f^2}{2\delta^2}}\, df \tag{23}$$

And C_0 is the clutter residue at the output of MTI filter which equal

$$C_0 = \int_0^{\infty} |H(f)|^2\, e^{\frac{-f^2}{2\delta^2}} df \tag{24}$$

For finding C_0, say

$$C_0 = \int_0^{\infty} (\frac{1}{3}\cos 4\pi Tf .e^{\frac{-f^2}{2\sigma^2}} df_d - \frac{4}{3}\int_0^{\infty} \cos 2\pi Tf .e^{\frac{-f^2}{2\sigma^2}} df_d + 3\int_0^{\infty} e^{\frac{-f^2}{2\sigma^2}} df_d + + \frac{2}{3}\int_0^{\infty} \cos 2\pi Tf \frac{M}{N}\cos 4\pi Tf e^{\frac{-f^2}{2\sigma^2}} df_d - \frac{8}{3}\int_0^{\infty} \cos 2\pi Tf \frac{M}{N}\cos 2\pi Tf \frac{M}{N}\cos 2\pi Tf e^{\frac{-f^2}{2\sigma^2}} df_d \tag{25}$$

By the aid of integration tables, these integrals were solved and the results are:

$$C_0 = \frac{1}{3}\bullet\frac{1}{2}\sqrt{2\pi}\,\sigma\; e^{-8(\pi T\sigma)^2} - \frac{4}{3}\bullet\frac{1}{2}\sqrt{2\pi}\sigma\; e^{-2(\pi T\sigma)^2} + 3\frac{1}{2}\sqrt{2\pi}\,\sigma + \frac{2}{3}\bullet\frac{1}{2}\sqrt{2\pi}\,\sigma\; e^{-2(\pi T\sigma)^2(4+\frac{M^2}{N^2})}.\cosh 8(\pi^2T^2\sigma^2)\frac{M}{N} \tag{26}$$

$$-\frac{8}{3}\bullet\frac{1}{2}\sqrt{2\pi}\,\sigma\; e^{-2(\pi T\sigma)^2(1+\frac{M^2}{N^2})}\cosh 4(\pi T\sigma)^2\frac{M}{N}$$

By applying the definition of improvement factor.

$$I = 3\frac{1/2\sqrt{2\pi}\sigma}{\frac{1}{2}\sqrt{2\pi}\sigma\left[\frac{1}{3}e^{-8(\pi T\sigma)^2} - \frac{4}{3}e^{-2(\pi T\sigma)^2} + 3 + \frac{2}{3}e^{-2(\pi T\sigma)^2(4+\frac{M^2}{N^2})}\cosh 8(\pi T\sigma)^2\frac{M}{N} - \frac{8}{3}e^{-2(\pi T\sigma)^2(1+\frac{M^2}{N^2})}\cosh 4(\pi T\sigma)^2\frac{M}{N}\right]}$$

Finally

$$I = \frac{1}{1+\frac{1}{9}e^{-8(\pi T\sigma)^2} - \frac{4}{9}e^{-2(\pi T\sigma)^2} + \frac{2}{9}e^{-(\pi T\sigma)^2(4+\frac{M^2}{N^2})}\cosh 8\,(\pi T\sigma)^2\frac{M}{N} - \frac{8}{9}e^{-2(\pi T\sigma)^2(1+\frac{M^2}{N^2})}\cosh 4(\pi T\sigma)^2\frac{M}{N}} \tag{27}$$

computer program has been done for (30) to indicate the improvement factor for three- period staggered as a function of standard deviation of clutter (σ) in (Hz). The results have drawn in figs (8) to (9).

ISSN 1533-9211

DOI 10.17605/OSF.IO/JRQA5

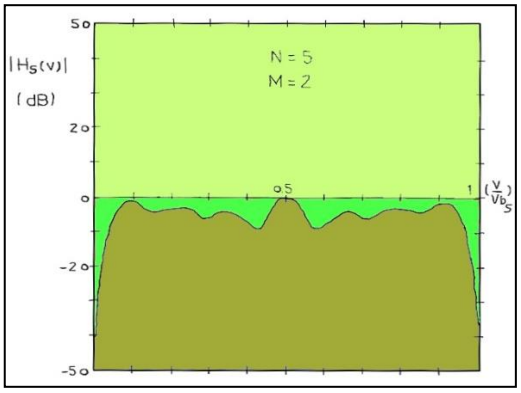

Figure 4: Velocity Response at Stagger Ratio 4:5:6

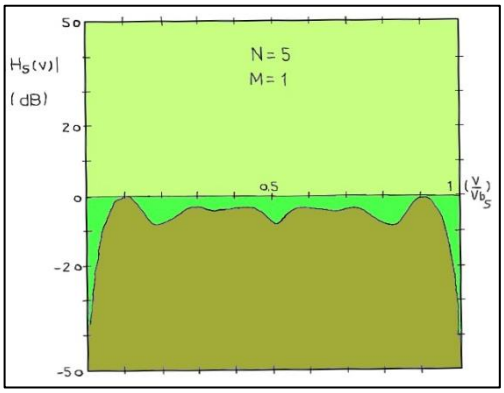

Figure 5: Velocity Response at Stagger Ratio 3:5:7

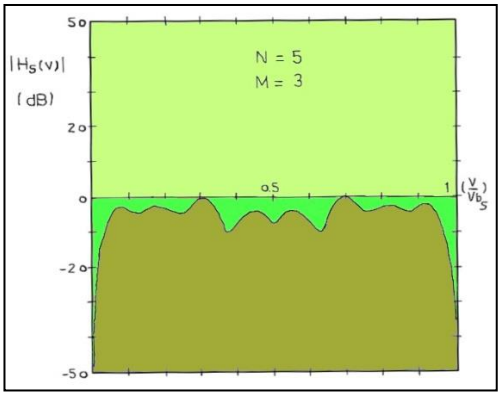

Figure 6: Velocity Response at Stagger Ratio 2:5:8

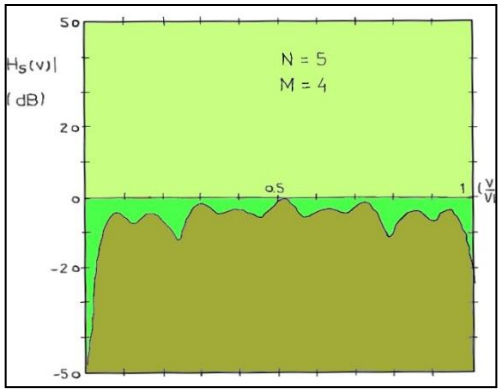

Figure 7: Velocity Response at Stagger Ratio 1:5:9

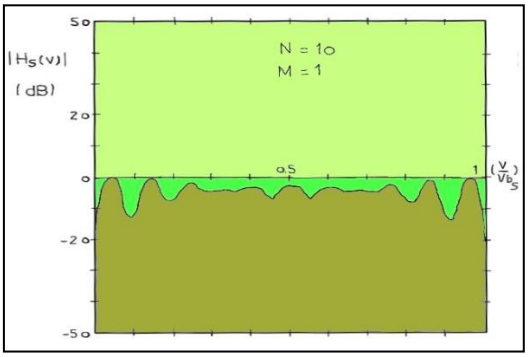

Figure 8: Velocity Response at Stagger Ratio 9:10:11

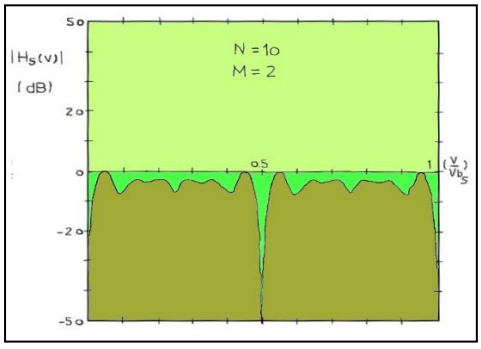

Figure 9: Velocity Response at Stagger Ratio 8:10:12

ISSN 1533-9211

DOI 10.17605/OSF.IO/JRQA5

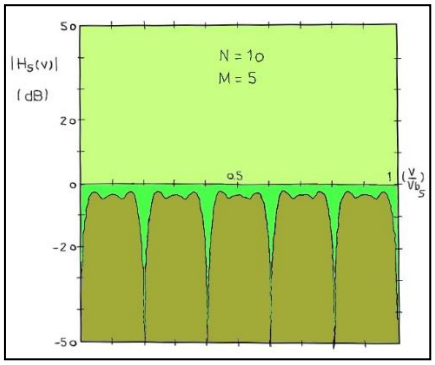

Figure 10: Velocity Response at Stagger Ratio 5:10:15

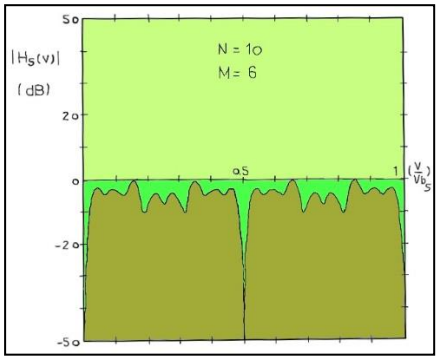

Figure 11: Velocity Response at Stagger Ratio 4:10:16

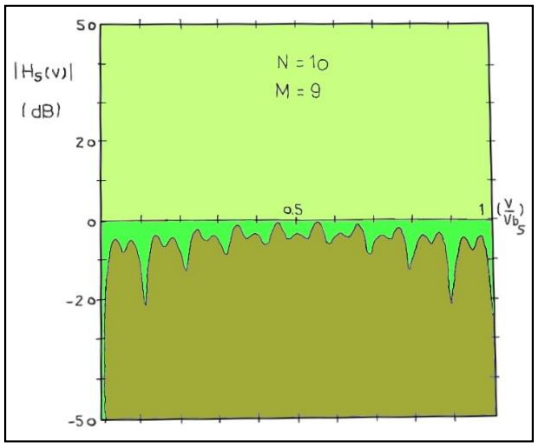

Figure 12: Velocity Response at Stagger Ratio 1:10:19

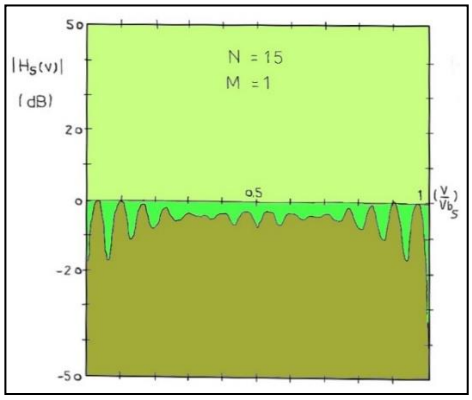

Figure 13: Velocity Response at Stagger Ratio 14:15:16

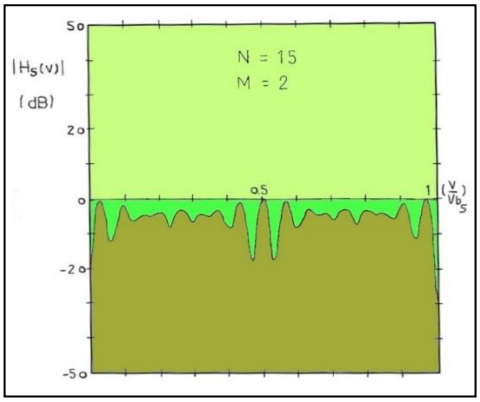

Figure 14: Velocity Response at Stagger Ratio 13:15:17

ISSN 1533-9211

DOI 10.17605/OSF.IO/JRQA5

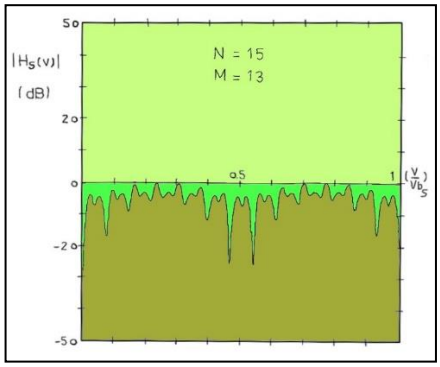

Figure 15: Velocity Response at Stagger Ratio 2:15:28

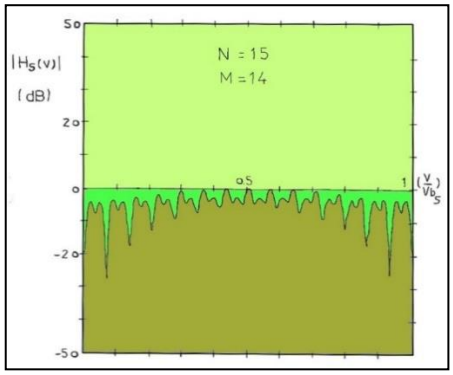

Figure 16: Velocity Response at Stagger Ratio 1:15:29

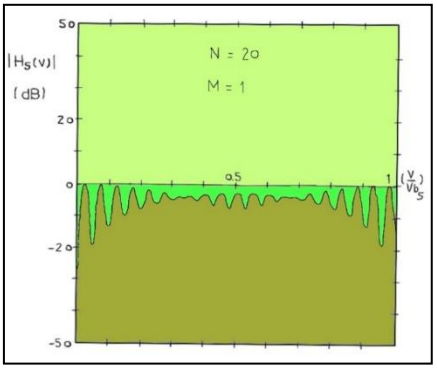

Figure 17: Velocity Response at Stagger Ratio 19:20:21

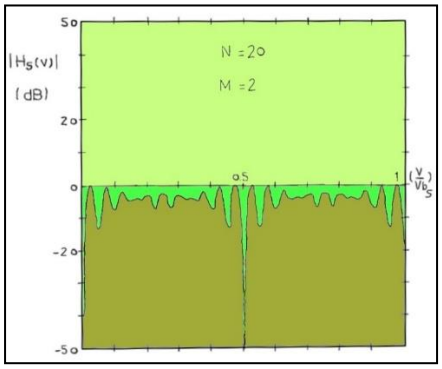

Figure 18: Velocity Response at Stagger Ratio 18:20:22

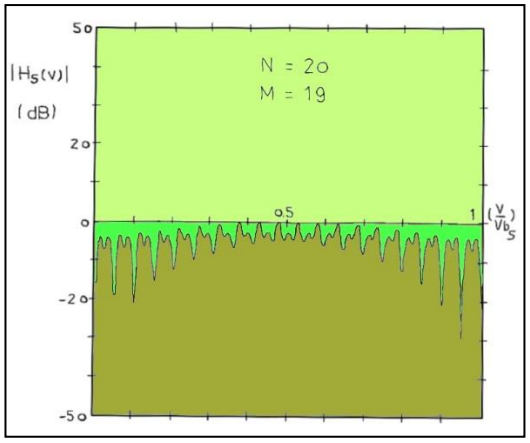

Figure 19: Velocity Response at Stagger Ratio 1:20:39

ISSN 1533-9211

DOI 10.17605/OSF.IO/JRQA5

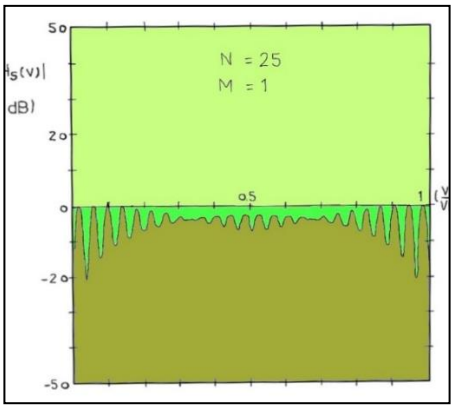

Figure 20: Velocity Response at Stagger Ratio 24:25:26

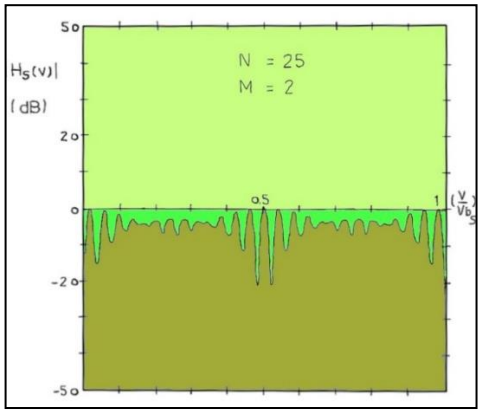

Figure 21: Velocity Response at Stagger Ratio 23:25:27

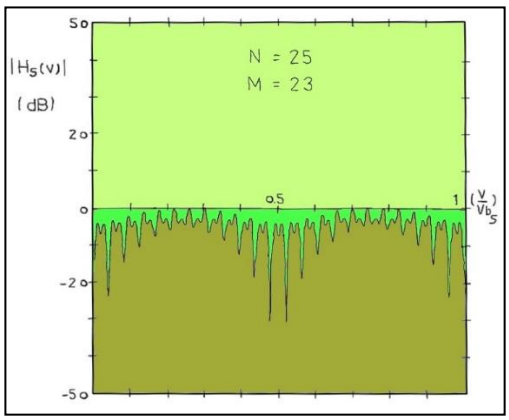

Figure 22: Velocity Response at Stagger Ratio 2:25:48

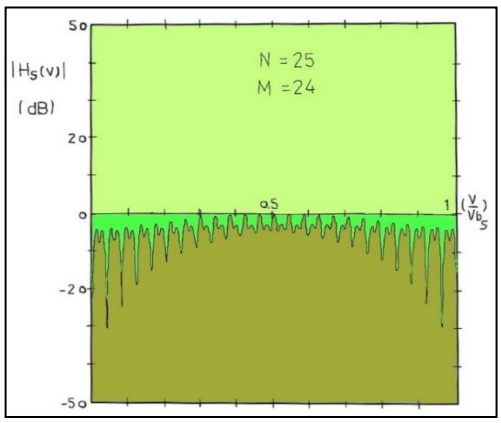

Figure 23: Velocity Response at Stagger Ratio 1:25:49

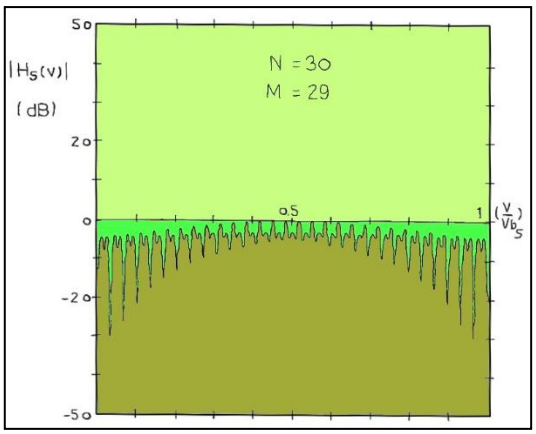

Figure 24: Velocity Response at Stagger Ratio 1:30:59

ISSN 1533-9211

DOI 10.17605/OSF.IO/JRQA5

Table 2: Velocity respons |Hs (v)| Vs staggered delay

				Velocity Respons | Hs(v)|
Staggered Delay (M)	Mean Period of Main Delay Line (N)	Staggered Ratio	No of Deepest Min.	Deepest Min. (dB)
1	5	4 : 5 : 6	3	- 8
2	5	3 : 5 : 7	2	- 9
3	5	2 : 5 : 8	2	- 10
4	5	1 : 5 : 9	2	- 12
1	10	9 : 10 : 11	2	- 13
5	10	25 : 10 : 15	4	- 50
6	10	4 : 10 : 16	1	- 50
9	10	4 : 10 : 19	2	- 20
1	15	14 : 15 : 16	2	- 26
13	15	2 : 15 : 28	2	- 28
1	20	19 : 20 : 21	2	- 18
2	20	18 : 20 : 22	1	- 50
19	20	1 : 20 : 39	2	- 30
1	25	24 : 25 : 26	2	- 22
23	25	2 : 25 : 48	2	- 30
24	25	1 : 25 : 49	2	- 30
29	30	1 : 30 : 59	2	- 30

Table 3: Velocity Respons |Hs (v)| Vs Staggered Delay

			Velocity Respons |Hs(v)|
Staggered Delay (M)	Mean Period of Main Delay Line (N)	No. of Deepest Min.	Deepest Min. (dB)
4	5	1	- 12
2 4 6 8	10	3	- 50
3 5 10	15	3	- 50
2.5 5 8 10 15 18	20	7	- 50
5 10 15 20	25	4	- 50
4 8 10 12 15 18 20 22 25 27	30	10	- 50

The Seybold Report
ISSN 1533-9211
DOI 10.17605/OSF.IO/JRQA5

CONCLUSION

Many of the recent sophisticated radar systems are characterized by the fact that they have to acquire and track small targets at large distances and at angles close to the horizon.

In order to meet these requirements, high radiated power levels and increased receiving system sensitivity are frequently required.

As a result, several problems arise which can severely limit radar performance while these problems are different in effect.

The mean period of the main delay line N= 5

It has been obtained that the depth of the deepest minimum is increased by increasing the staggered ratio, four values for the staggering delay has been used, i.e., from (1-4) the value of response voltage characteristics is increased from (-8 to - 12 dB) and the position of deepest minimum is changed (i.e., when the staggered delay (M) is 1). The deepest minimum was the first blind speed, but when the staggered delay goes further. The deepest minimum changed their position as shown in Figs (4) to (7)

The mean period of the main delay line 'N=10

In this case when the value of staggered delay (M) is (1), it has been obtained that the deepest minimum is the first blind speed and his value is (-14dB). But, when the staggered delay (M) increased to (2), we have got a deepest minimum with a value of (-50dB) in the middle of response curve, and if (M) increased more, the position of the first blind speed is changed.

It has been noticed that when mean period of main delay line (N) is an even number a deepest minimum with a value of (-50dB) appeared in the response curve, but if the staggered ratio is 1/2, the worst case for staggering has been obtained because it has got many deepest minimum in response curve all with a voltage response of (-50dB) Fig. (8). But the best case for staggering is when M=N-1 Fig. (10)

The mean period of the main delay line N= 15

In this case when the staggered delay (M is 1) the deepest minimum was the first blind speed with voltage response value of (-17dB) Fig. (14), a worst case has been obtained at a staggered ratio (1/3, 2/3, 1/5, 2/5, and 3/5) but the best case when M = N-1 Fig. (17).

The mean period of main delayi line N=20

The deepest minimum his occurred in this case when the staggered delay (M) is an even number, the depth of the deepest minimum in the response curve is (-19dB). Fig. (18), and the worst cases were the staggered ratio (1/5, 2/5, 3/5,4/5, 1/2,1/4 and 3/4), but the best case when M=N-1 Fig. (20).

The mean period of main delay line' N = 25

It has been noticed in this case that, if the staggered delay (M) is (1), the depth of the deepest min. in the response curve iš (-22dB). Fig. (21), but the worst case has occurred when the

The Seybold Report
ISSN 1533-9211
DOI 10.17605/OSF.IO/JRQA5

staggered ratio is (1/5, 2/5, 3/5 and 4/5) with a value of voltage response is equal (-50dB). The best case when M=N-1 Fig. (24).

The mean period of main delay line N=30

It has been obtained in this case that when the staggered delay (M) is an even number, the deepest minimum with a response voltage equal (-50dB) in the response curve has occurred, but the worst case is when the staggered ratio is (1/6, 1/3, 1/2, 2/7 and 5/6). The best case when (M= N-1) Fig. (22).

The deepest minimum for each case, i.e., when the mean period of main delay line (N) is (5, 10, 15, 20, 25 and 30), were plotted as a function of staggered delay (M). Fig. (25) to (30), which shows the effect of the odd and the even numbers upon the staggering.

References

1) Knott, Eugene F., John F. Schaeffer, and Michael T. Tulley. Radar cross section. SciTech Publishing, 2004.

2) Martone, Anthony F., Kenneth Ranney, and Calvin Le. "Noncoherent approach for through-the-wall moving target indication." IEEE Transactions on Aerospace and Electronic Systems 50.1 (2014): 193-206.

3) Zuyin, Weng. "Optimal design of clutter rejection filters for MTI system." 2001 CIE International Conference on Radar Proceedings (Cat No. 01TH8559). IEEE, 2001.

4) Martone, Anthony, Kenneth Ranney, and Roberto Innocenti. "Through-the-wall detection of slow-moving personnel." Radar Sensor Technology XIII. Vol. 7308. SPIE, 2009.

5) He, Qian, et al. "MIMO radar moving target detection in homogeneous clutter." IEEE Transactions on Aerospace and Electronic Systems 46.3 (2010): 1290-1301.

6) Zuyin, Weng. "Optimal design of clutter rejection filters for MTI system." 2001 CIE International Conference on Radar Proceedings (Cat No. 01TH8559). IEEE, 2001.

7) Bounaceur, Hamza, Ali Khenchaf, and Jean-Marc Le Caillec. "Analysis of small sea-surface targets detection performance according to airborne radar parameters in abnormal weather environments." Sensors 22.9 (2022): 3263.

8) Slob, Evert, Motoyuki Sato, and Gary Olhoeft. "Surface and borehole ground-penetrating-radar developments." Geophysics 75.5 (2010): 75A103-75A120.

9) Knott, Eugene F. Radar cross section measurements. Springer Science & Business Media, 2012.

10) Seltmann, Jörg EE. "Weather Radar." Springer Handbook of Atmospheric Measurements. Springer, Cham, 2021. 841-900.

11) Martin, Jack. "High-volume manufacturing and field stability of MEMS products." Springer Handbook of Nanotechnology. Springer, Berlin, Heidelberg, 2010. 1803-1833.

12) Martin, Jack. "High-volume manufacturing and field stability of MEMS products." Springer Handbook of Nanotechnology. Springer, Berlin, Heidelberg, 2010. 1803-1833.

13) Dobkin, Bob, and Jim Williams, eds. "Analog circuit design: a tutorial guide to applications and solutions." (2011).

14) Astakhov, Viktor P. Geometry of single-point turning tools and drills: fundamentals and practical applications. Springer Science & Business Media, 2010.

The Seybold Report
ISSN 1533-9211
DOI 10.17605/OSF.IO/JRQA5

15) Singh, Abhinav, Vaibhav Shah, and Anurag Sarnaik. "Moving Target Indication Radar." International Journal of (2013).

16) Stanton, Timothy K., Wu-Jung Lee, and Kyungmin Baik. "Echo statistics associated with discrete scatterers: A tutorial on physics-based methods." The Journal of the Acoustical Society of America 144.6 (2018): 3124-3171.

17) Zia, Roseanna N. Individual particle motion in colloids: Microviscosity, microdiffusivity, and normal stresses. California Institute of Technology, 2011.

18) Scherer, Sebastian, Lyle Chamberlain, and Sanjiv Singh. "Autonomous landing at unprepared sites by a full-scale helicopter." Robotics and Autonomous Systems 60.12 (2012): 1545-1562.

19) Fulton, Caleb, et al. "Cylindrical polarimetric phased array radar: Beamforming and calibration for weather applications." IEEE Transactions on Geoscience and Remote Sensing 55.5 (2017): 2827-2841.

20) Atzeni, C., et al. "Early warning monitoring of natural and engineered slopes with ground-based synthetic-aperture radar." Rock Mechanics and Rock Engineering 48.1 (2015): 235-246.

21) Kavitha, L. Babu Saraswathi, and I. Jacob Raglend. "A wide-scan phased array antenna for a small active electronically scanned array: a review." 2013 International Conference on Circuits, Power and Computing Technologies (ICCPCT). IEEE, 2013.

22) Schvartzman, David, Sebastián M. Torres, and Tian-You Yu. "Motion-compensated steering: Enhanced azimuthal resolution for polarimetric rotating phased array radar." IEEE Transactions on Geoscience and Remote Sensing 59.12 (2021): 10073-10093.

23) Weierstall, Uwe, J. C. H. Spence, and R. B. Doak. "Injector for scattering measurements on fully solvated biospecies." Review of Scientific Instruments 83.3 (2012): 035108.

24) Mounaix, Mickael, et al. "Spatiotemporal coherent control of light through a multiple scattering medium with the multispectral transmission matrix." Physical review letters 116.25 (2016): 253901.

25) Swindlehurst, A. Lee, et al. "Applications of array signal processing." Academic Press Library in Signal Processing. Vol. 3. Elsevier, 2014. 859-953.

26) Fox, Zachary W., et al. "Implementation of continuous fast scanning detection in femtosecond Fourier-transform two-dimensional vibrational-electronic spectroscopy to decrease data acquisition time." Review of Scientific Instruments 89.11 (2018): 113104.

27) Cui, Kaihua, et al. "Scanning error detection and compensation algorithm for white-light interferometry." Optics and Lasers in Engineering 148 (2022): 106768.

28) Cui, Kaihua, et al. "Scanning error detection and compensation algorithm for white-light interferometry." Optics and Lasers in Engineering 148 (2022): 106768.

29) Chen, Xiaolong, et al. "Detection and extraction of target with micromotion in spiky sea clutter via short-time fractional Fourier transform." IEEE Transactions on Geoscience and Remote Sensing 52.2 (2013): 1002-1018.

30) Narbudowicz, Adam, Max J. Ammann, and Dirk Heberling. "Switchless reconfigurable antenna with 360° steering." IEEE Antennas and Wireless Propagation Letters 15 (2016): 1689-1692.